Separation Science and Technology
Publication details, including instructions for authors and subscription information:
http://www.informaworld.com/smpp/title~content=t713708471

Fouling of Thin-Channel and Tubular Membrane Modules by Dilute Suspensions

S. Ilias[a]; R. Govind[a]
[a] Department of Chemical Engineering, University of Cincinnati, Cincinnati, Ohio

To cite this Article Ilias, S. and Govind, R.(1988) 'Fouling of Thin-Channel and Tubular Membrane Modules by Dilute Suspensions', Separation Science and Technology, 23: 12, 1753 — 1771
To link to this Article: DOI: 10.1080/01496398808075661
URL: http://dx.doi.org/10.1080/01496398808075661

SEPARATION SCIENCE AND TECHNOLOGY, 23(12&13), pp. 1753-1771, 1988

FOULING OF THIN-CHANNEL AND TUBULAR MEMBRANE MODULES BY DILUTE SUSPENSIONS

S. Ilias and R. Govind*
Department of Chemical Engineering
University of Cincinnati
Cincinnati, Ohio 45221

ABSTRACT

In this paper, fouling of thin-channel and tubular ultrafiltration (UF) membrane modules by dilute suspensions have been studied theoretically. A hydrodynamic analysis of fluid-particle system is presented to describe the role of dilute suspensions in fouling such membrane modules. The present analysis assumes that for very dilute suspensions, only inertial effects are important for particulate fouling. Particle trajectory history and hence the fouling is computed from equations of motion for the particles, where the fluid-flow is given by the full solution of Navier-Stokes equation . To simulate the flux decline due to build up of foulant layer on the membrane walls, it is assumed that the deposition of particles on the membrane surface at discrete time interval is a steady state event and thus formulating the fouling problem as an infinite series of successive steady state events. Present simulation results indicate that inertial effects are important and under positive wall permeation flux conditions, particles are encouraged to migrate towards the membrane wall causing so-called *'membrane fouling'* by the particulates.

INTRODUCTION

Ultrafiltration (UF) is a pressure-driven membrane process which deals with separation of fairly large molecules, colloidal and particulate suspensions. In recent years, the UF membrane process has gained considerable importance in many industrial applications due to its low energy requirement, athermal character and improved

* To whom correspondence should be addressed.

membrane properties and module design. Ultrafiltration membranes currently find their greatest use in the processing of food and dairy products, the recovery of electrophoretic paints and in the biotechnology oriented applications such as the harvesting of microbial cells, fractionation of fermentation broths and high performance reactors for enzymatic and fermentation processes (*1*). However, the present UF membrane processes for liquid feed streams are complicated by the phenomena of *membrane fouling* and of *concentration polarization* in the liquid boundary layer adjacent to the membrane wall.

Fouling seems to result from deposition and accumulation of suspended and colloidal particles on the membrane surface, and/or the crystallization and precipitation or adsorption of smaller solutes and macromolecules on the surface and within the pore strucures of the membrane (*2,3*). Thus, membrane fouling manifests the result of simultaneous combination and/or interaction of several factors, which may include membrane surface chemistry, solute-fluid, solute-solute and solute membrane interactions. On the other hand, concentration polarization is a build-up of rejected solutes near the membrane surface. This build-up is caused by the limitations on the rate at which the rejected solute can be transported back into the bulk of the solution by diffusion or other processes *(4)*.

The various factors that need to be addressed in developing a comprehensive model to describe membrane fouling in UF process containing dilute suspensions and macromolecules, is shown schematically in Figure 1. An attempt to include all these factors in a working model may appear attractive, but mathematically the development of a physical model of such magnitude is a formidable task. However, to simplify the problem, the fouling phenomena may be visualized as a two step process. The first step includes the hydrodynamic interactions (far field effects) which dictate the conditions under which a particle or suspended colloid would migrate towards the membrane surface. The second step is governed by the surface forces, chemical and electrokinetic interactions (near field effects), which are dominant near the membrane surface, and play a role in fouling when the particles and the colloids are within the zone of near field effects (*5,6*).

There are number of models that describe the flux decline due to fouling and concentration polarization in UF membranes *(3,7,8,9)*. Predictive models for flux decline have tended to use semi-empirical deposition kinetics (usually 1st order reaction) to calculate the increase in resistance due to build up of fouling layer *(3,7)*. The other class of models are convective mass transfer models, known as *"concentration polarization model"* and have been widely used in predicting flux reduction. In membrane processes large solute molecules and particles are rejected by the membrane. This results in developing a viscous and gelatinous layer on the membrane surface which gives new resistance in addition to those of membrane wall and the concentration boundary layer *(8,9)*. There are models which account for the precipitation of solutes on the membrane surface in the concentration polarization model *(10)*. Here, the mass transfer processes causing concentration polarization and precipitation kinetics are coupled, since the rate of precipitation is a function of solute concentration.

In modeling membrane fouling by dilute suspensions, the trend has been to ignore the role of hydrodynamic interactions , which is assumed to be unimportant or too complex to incorporate into a working model. In recent years, Belfort et al., *(5)* and Kleinstreuer and Belfort *(6)*, studied the hydrodynamics of dilute suspensions in fouling UF membrane modules. From their theoretical and experimental studies on the migration of single particles in a thin-channel with one permeable wall, it was concluded that the permeation drag and inertial lift force play an important role. Under favorable conditions, particles migrate due to inertial forces to membrane surface and

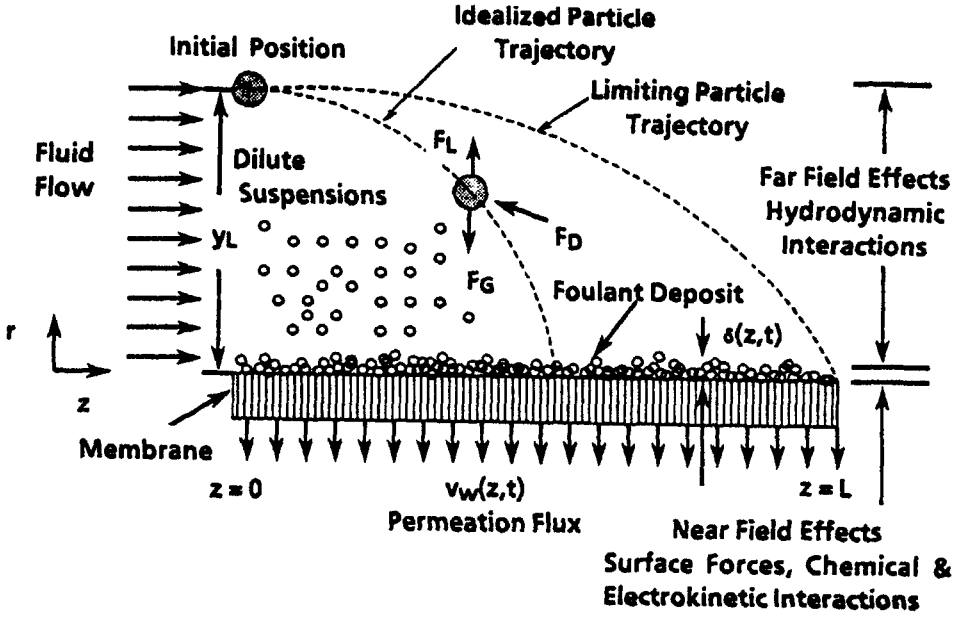

Figure 1: Flow of dilute suspensions in a permeable membrane showing various factors needed to develop a comprehensive model.

result in membrane fouling. To quantify the membrane fouling by particulates, recently the authors modeled the fouling problem based on hydrodynamics of fluid-particle systems and presented steady state particle deposition fluxes on a tubular UF membrane module *(11)*. In this paper, our previous work on steady state membrane fouling is extended to model the initial flux decline in thin-channel and tubular UF membrane modules. As the macromolecules and particles deposit on the membrane surface as a foulant layer, the layer builds up with time which adds additional resistance to the permeate flow. The flux decline is modeled by assuming that at a discrete time interval, the particle deposition process is a steady state event and thus formulating the fouling as an infinite series of such successive events. The analysis stresses the importance of far field effects which contribute to the migration and deposition of colloidal and suspended particles on membrane surface, causing so called *'fouling'* by the particulates.

THEORETICAL DEVELOPMENT

Consider a tubular UF membrane module across which flows a Newtonian fluid containing a dilute suspension of rigid neutrally buoyant particles. The transmembrane pressure is such that the particles are retained within the membrane module but the product (pure fluid) permeates across the membrane at a permeation velocity, v^*_w, which in general is a function of particle layer, h', membrane permeability, A and

transmembrane pressure, p^*. Since both h^* and p^* vary with axial position, z^*, then v^*_w is also a function of axial position. As the foulant layer grows, v^*_w varies with time. Our objective is to compute v^*_w and h^* from known quantities, such as initial inlet feed concentration, inlet transmembrane pressure and module geometry. For this we need to know the fluid flow field and the movement of particles in the module, which is obviously a complex problem. The problem is simplified by making the following assumptions:

- Laminar and incompressible flow
- Membrane permeation rates are small as compared with the axial velocity
- Particle concentration is so low that the particles do not disturb the fluid flow and may be taken independent of the other
- Particle-particle, particle-membrane interactions are neglected
- The osmotic effects are neglected as being small in UF processes
- The permeability of deposited particle layer is constant

Based on the above assumptions, the appropriate governing equations in normalized form (symbols are defined in the Nomenclature) for the fluid phase are given by the equations of motion and continuity, equations (1) and (2). For particles motion, the axial and radial components of equations of motion for the particles, are given by equations (3) and (4), respectively. The analysis that follows can be easily extended to the case of thin-channel UF membrane modules and hence we will not repeat it here.

$$\frac{\partial u^*}{\partial t^*} + u^* \frac{\partial u^*}{\partial z^*} + v^* \frac{\partial u^*}{\partial r^*} = \frac{dp^*}{dz^*} + \frac{\partial^2 u^*}{\partial r^{*2}} + \frac{1}{r^*} \frac{\partial u^*}{\partial r^*} \tag{1}$$

$$r^* \frac{\partial u^*}{\partial z^*} + \frac{\partial}{\partial r^*}(v^* r^*) = 0 \tag{2}$$

$$\frac{d^2 z^*}{dt^{*2}} = -\frac{3 C_D Re_p}{16} (\rho/\rho_p)(d/d_p)^2 \left(\frac{dz^*}{dt^*} - u^* \right) \tag{3}$$

$$\frac{d^2 r^*}{dt^{*2}} = -\frac{3 C_D Re_p}{16} (\rho/\rho_p)(d/d_p)^2 \left(\frac{dr^*}{dt^*} - v^* \right) \tag{4}$$

The appropriate boundary conditions for equations (1-2) are:

$$u^*(r^*,0) = U_0^*(r^*); \qquad v^*(r^*,0) = 0$$

$$\frac{\partial u^*}{\partial r^*}(0,z^*) = 0; \quad u^*(1,z^*) = 0; \quad v^*(1,z^*) = v_w^* = A p^* \text{ or } Constant$$

The boundary conditions for equations of motion for the particles, equations (3-4) are:

$$at \ t^* = 0 \qquad u_p^*(r^*,z^*) = u^*(r^*,z^*); \qquad v_p^*(r^*,z^*) = v^*(r^*,z^*)$$

As a particle layer deposits on the membrane wall, the membrane permeability, A, varies with time, which is not known before hand. Also there may be compaction of the deposited cake layer and membrane pore blockage, which may add to this problem. To simplify this, we viewed the build-up of foulant layer on the membrane surface for a short interval of time as a steady state event and formulated the fouling problem as an infinite series of such events. Therefore, at each discrete time interval, equations (1) and (2) are solved as a steady flow problem in a permeable tube. The solution of equations (3) and (4) along with the fluid flow given by equations (1) and (2), will give a deterministic

picture of particle trajectory history for the given boundary conditions. Based on the particle trajectory information, a simple input-output balance of particles can be formulated to compute the particle deposition flux. For example, a particle starting at the inlet section of the membrane module (r^*,0) may be captured on the membrane wall at some axial position (1,z^*). Then it may be shown that all particles within a differential element dr^* at the inlet section would be mapped on a differential axial element dz^*, provided that the element dr^* is within the limiting trajectory range. Thus a simple differential material balance will give:

$$2\pi C_0^* U_0^*(r^*) r^* dr^* = 2\pi \Gamma(z^*) dz^* \tag{5}$$

where $\Gamma(z^*)$ is the particle deposition flux, C_0^* and $U_0^*(r^*)$ are normalized inlet particle concentration and fluid velocity profile, respectively. If the inlet particle concentration isassumed uniform ($C_0^* = 1$) and the velocity profile is parabolic, then equation (5) may be rearranged to give the particle deposition flux as:

$$\Gamma\Big|_{z^*} = 2r^*(1 - r^{*2})\frac{dr^*}{dz^*} \tag{6}$$

Equation (6) may now be integrated with appropriate limits to obtain the total particle deposition rates over the range of interest.

As time progresses, the flow of permeate through the membrane declines due to added resistance caused by the particle layer deposited on the membrane surface. To compute the new resistance in addition to the membrane resistance, as mentioned earlier, at each discrete time the deposition of particle is viewed as a steady state event. Thus, for example, in time Δt^*, one may obtain the amount of particle deposits and average thickness of the deposited layer. Once the deposition rates are known from equation (6), the amount of cake deposited in time Δt^*, on a membrane module of length z^*, becomes,

$$\overline{m} = \Delta t^* \int_0^{z^*} \Gamma(z^*) dz^* \tag{7}$$

If h' is the thickness of foulant layer, having permeability k', then the resistance of this layer is given by *(7)*:

$$R_f = \frac{\nu^2 h'}{k' H U_{0,m}^2} \tag{8}$$

where permeability of the cake layer, k' may be approximated from the widely used Kozeny-Carman equation for porous solids of porosity, ε *(4)*:

$$k' = \frac{d_p^2}{180}\frac{\varepsilon^3}{(1-\varepsilon^2)} \tag{9}$$

Thus, a new wall permeation flux at the end of Δt^*, time-step i.e. at $t^* = t^* + \Delta t^*$, can be computed by assuming that the resistances of the membrane, R_m ($R_m = 1/A$) and cake layer, R_f are in series. Then the new wall flux condition becomes *(7)*,

$$v_w^* = \frac{p^*}{R_m + R_f} \tag{10}$$

With new flux condition, the solution procedure for fluid-flow and particles are advanced for time increment Δt^* and the new values of h' and k' are computed as time progresses. An implicit assumption in this analysis is that each deposited cake layer at

discrete time intervals has the same porosity and hence the same permeability. Also it is assumed the thickness of the cake layer is so small that the effective flow passage in the membrane module remains unchanged.

COMPUTATIONAL SCHEMES

The equations for fluid-flow, equation (1-2) with appropriate boundary conditions are solved by a finite difference method implicit in r^*. The numerical details are reported elsewhere for a tubular UF membrane module *(11)*, which may be easily extended to thin-channel membrane modules. Here, a brief outline of the solution procedure will be given. The governing equations are written by finite difference approximation at each discretized grid points as a set of linear algebraic equations, represented by a tridiagonal matrix and solved by the well known Thomas Algorithm. For convergence, an iterative scheme is implemented where the pressure gradient, dp^*/dz^* is guessed and the solution procedure is iterated till the wall permeation flux condition is satisfied according to the preset tolerance limit. Grid spacings in the axial and radial directions are established by grid independency tests.

The equations of motion for particles, equations (3-4) are solved by Fourth-order Runge-Kutta method, where the solution of fluid-flow have been used to compute fluid-particle slip velocities. The solution gives the particle trajectory history. The particle deposition flux is calculated from the limiting particle trajectory via equation (6).

As outlined in the previous section, to predict the flux decline with time, the equations for fluid-flow and particle trajectories are solved again with new values of wall permeation flux condition, at each discrete time interval, Δt^*, exactly by the same method as described above. The time step, $\Delta t^* = 0.05$, was used in computing flux decline. The time step was established by numerical experimentation, such that the flux decline remain essentially unchanged for any values of $\Delta t^* < 0.05$.

RESULTS AND DISCUSSION

In this paper, we analysed the hydrodynamics of dilute suspensions and its role in fouling thin-channel and tubular membrane modules. The governing equations for fluid-flow and particle motion are solved numerically for various wall flux conditions. Fluid-flow equations are solved for the case of fully developed flow at the entrance region (parabolic inlet profile). Permeate flux decline and particle deposition rates are computed to show how the build up of particle layer on the membrane surface affect the performance of UF modules. Here, we will briefly describe our simulation results in two major sections, e.g. fluid-flow and particulate fouling in UF modules.

Fluid-flow in Thin-channel and Tubular UF Membrane Modules:

A summary of test cases that have been studied are given in Table 1, with appropriate boundary conditions along with remarks on flow characteristics for thin-channel and tubular UF modules. Since the governing equations are solved in normalized form and consistent with initial assumptions, the fluid-flow results are applicable for all inlet flow conditions and fluid properties as long as the flow is laminar and incompressible.

The input data and model geometry that have been used in numerical simulation of fluid-flow and membrane fouling are tabulated in Table 2. In this study, the maximum length of computational domain (module axial length) used is $z^* = 0.2$, which corresponds to a length of $z = 14.5$ cm, based on the fluid properties and module dimension as given in Table 2.

Table 1: Summary of Test Cases Studied

Wall Boundary Conditions	Inlet Velocity Profile	Module Geometry	Remarks
$v^*_w = 0.1$	Parabolic	Thin-channel	Δp^* decreases with z^*
		Tubular	Δp^* decreases with z^*
$v^*_w = 1.0$	Parabolic	Thin-channel	Δp^* decreases with z^*
		Tubular	Δp^* decreases with z^*
$v^*_w = 3.0$	Parabolic	Thin-channel	Δp^* increases with z^*
		Tubular	Flow reversal, Δp^* & v^*_w increases
$A = 0.1$, $p^*_{inlet} = 1$	Parabolic	Thin-channel	Δp^* & v^*_w decreases with z^*
		Tubular	Δp^* & v^*_w decreases with z^*
$A = 1.0$, $p^*_{inlet} = 1$	Parabolic	Thin-channel	Δp^* & v^*_w decreases with z^*
		Tubular	Δp^* & v^*_w decreases with z^*
$A = 3.0$, $p^*_{inlet} = 1$	Parabolic	Thin-channel	Δp^* & v^*_w increases with z^*
		Tubular	Flow reversal, Δp^* & v^*_w increases

Table 2: Input Data and Dimensions of Membrane Module

Viscosity of fluid (g/cm s)	8.6×10^{-3}	Particle to module dia. ratio	4×10^{-4}
Density of fluid (g/cm^3)	1.0	Particle to fluid density ratio	1.59
Channel height or tube dia. (cm)	0.25	Inlet particle conc. (g/cm^3)	1.65×10^{-2}
Inlet avg. fluid velocity (cm/s)	10	Porosity of cake layer,	0.51, 0.30, 0.15
Maximum length of computational domain, z^*		0.20	
Flux decline computed for time, t^*		2.00	

In Figure 2(a,b), the normalized axial velocity profiles for various axial positions in a tubular UF module is shown for two representative wall permeation flux conditions of $v^*_w = 3.0$ and $A \times p^*_{in} = 3 \times 1$, respectively. At these wall flux conditions, along the increasing axial position, the axial velocity increases in central region of the tube. To compensate this increased axial flow, there is a decrease in velocity gradient near the permeable wall which shows the approach to a "separation profile". In this region, as shown in Figure 2(a) and (b), velocity profiles exhibit reverse flow at the wall at locations far from the inlet. However, for the variable wall permeation flux condition ($A \times p^*_{in} = 3 \times 1$), the separation profile appears much closer to the inlet as compared with that of constant wall flux condition ($v^*_w = 3.0$), which is due to increasing permeation rates along the axial position for the former case.

The development of axial velocity profiles in thin-channel UF module is shown in Figure 3(a,b) for wall flux conditions of $v^*_w = 3.0$ and $A \times p^*_{in} = 3 \times 1$, respectively. For both cases, in the computed axial domain, there is no appearence of separation profiles. It may be observed in Figure 3(a) and (b), the velocity profiles in the axial direction deviate from the parabolic inlet profile along the axial position. However, this deviation is more pronounced for the variable wall flux condition as compared with that of constant wall flux condition, as shown in Figure 3.

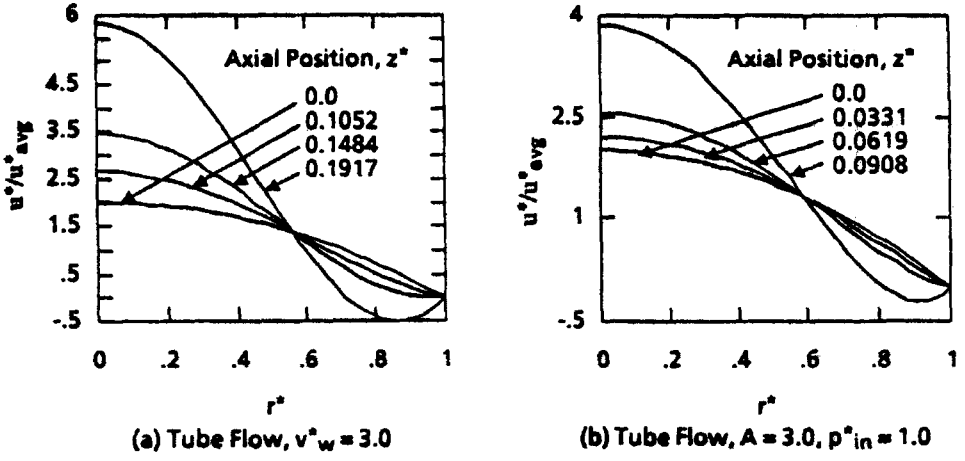

Figure 2: Dimensionless axial velocity profiles at different axial position in a tubular UF membrane module with fully developed inlet flow and wall flux conditions, (a) $v^*_w = 3$, (b) $v^*_w = A \times p^*_{in} = 3 \times 1$.

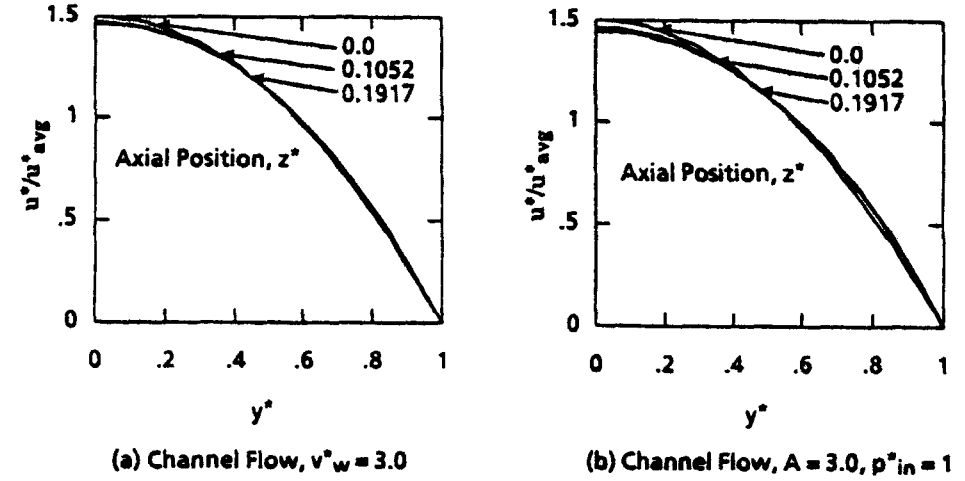

Figure 3: Dimensionless axial velocity profiles at different axial position in a thin-channel UF membrane module with fully developed inlet flow and wall flux conditions, (a) $v^*_w = 3$, (b) $v^*_w = A \times p^*_{in} = 3 \times 1$.

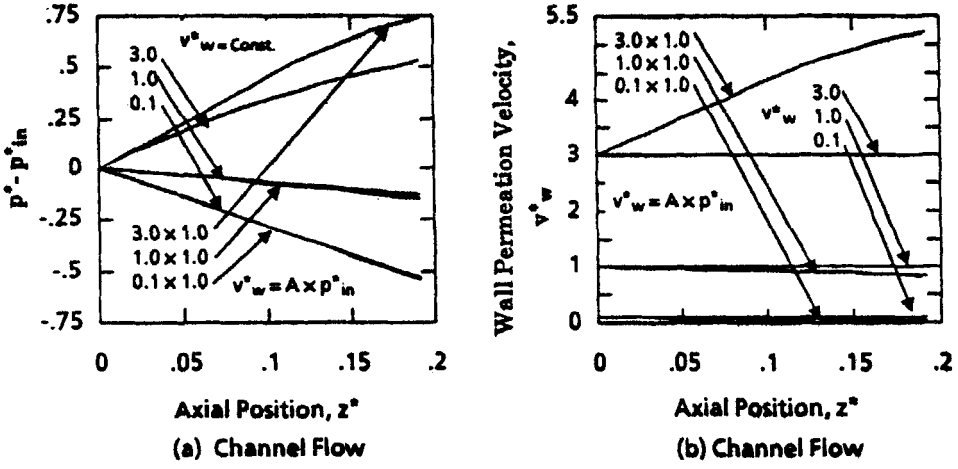

Figure 4: Variation of (a) dimensionless pressure, and (b) permeate flow rates along axial length in thin-channel UF module with fully developed inlet profile and various wall flux conditions.

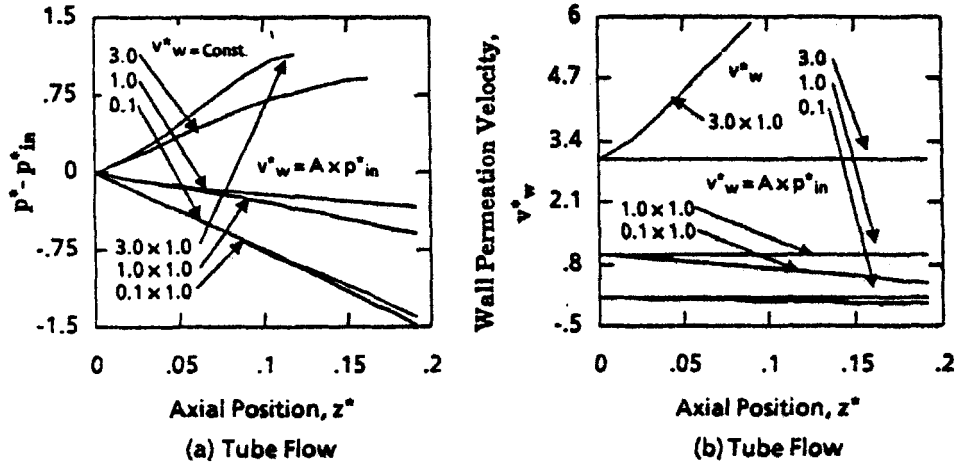

Figure 5: Variation of (a) dimensionless pressure, and (b) permeate flow rates along axial length in tubular UF module with fully developed inlet profile and various wall flux conditions.

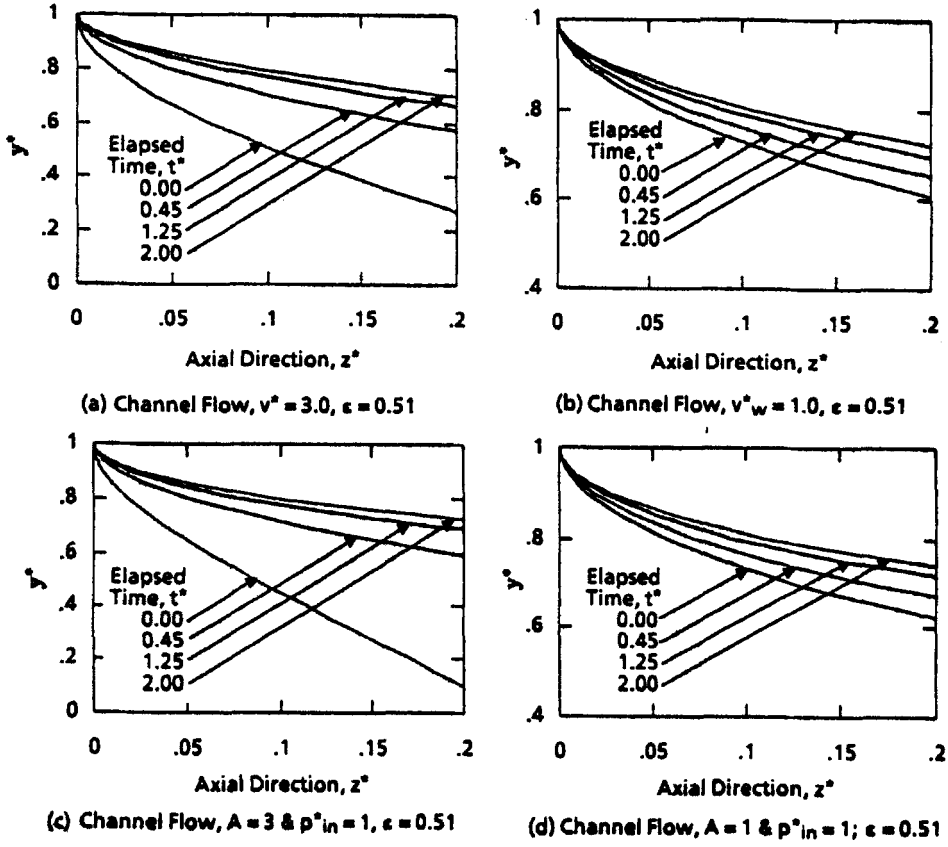

Figure 6: Locus of limiting particle trajectories in a thin-channel UF module (Membrane wall, $y^*=1$; Centerline, $y^*=0$) at various time with fully developed inlet profile and initial flux conditions, (a) $v^*_w=3$, (b) $v^*_w=1$, (c) $v^*_w=A\times p^*_{in}=3\times 1$, and (d) $v^*_w=A\times p^*_{in}=1\times 1$. Cake porosity, $\varepsilon=0.51$.

The variation of dimensionless pressure ($p^*-p^*_{in}$) and wall permeation velocity, v^*_w along the axial position for various wall boundary conditions in thin-channel and tubular UF membrane modules are shown in Figure 4(a,b) and 5(a,b), respectively. For both modules, at high wall permeation flux condition ($v^*_w=3.0$ and $A\times p^*_{in}=3\times 1$), the dimensionless pressure increases along the axial direction. The pressure recovery experienced by the flow at these high wall flux conditions, results in flow separation and reversal at the membrane wall as shown in Figure 2(a,b). At low wall flux condition

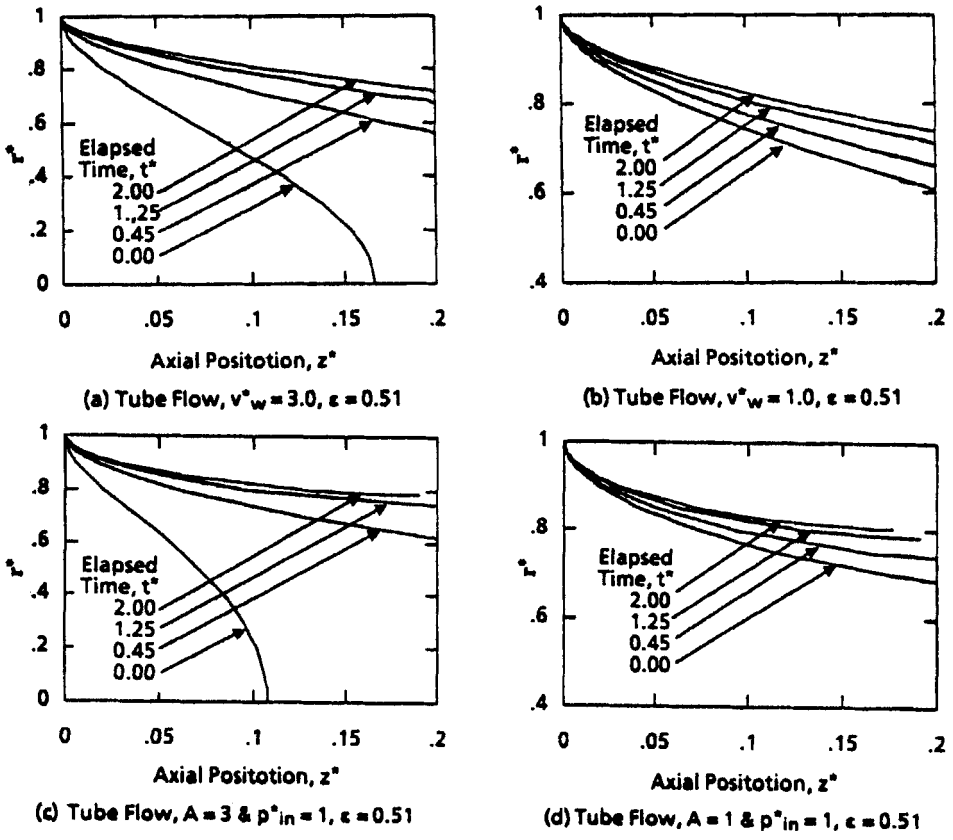

Figure 7: Locus of limiting particle trajectories in a tubular UF module (Membrane wall, $r^*=1$; Centerline, $r^*=0$) at various time with fully developed inlet profile and initial flux conditions, (a) $v^*_w=3$, (b) $v^*_w=1$, (c) $v^*_w=A\times p^*_{in}=3\times 1$, and (d) $v^*_w=A\times p^*_{in}=1\times 1$. Cake porosity, $\varepsilon=0.51$.

($v^*_w=1$, 0.1 and $A\times p^*_{in}=1\times 1$, 0.1×1), the dimensionless pressure decreases along the axial direction. The wall permeation velocity v^*_w, increases at high inlet wall flux condition ($A\times p^*_{in}=3\times 1$) and decreases at low inlet wall flux conditions ($A\times p^*_{in}=1\times 1$, 0.1×1) along the axial direction for both modules. With constant wall flux, which is due to imposed wall permeation velocity, remains constant along the axial length of the modules.

It is to be noted that at lower wall permeation flux conditions (both constant and variable inlet wall flux conditions), the pressure ($p^*-p^*_{in}$) and velocity(v^*_w) profiles do

not differ significantly from each other, which is also true for axial velocity profiles. However, for the same size and dimension of UF modules, at lower wall flux condition, a thin-channel module will follow closely the profiles of a fully developed channel-flow.

Fouling in Thin-channel and Tubular UF Membrane Modules:

In Figures (6) and (7), the locus of limiting particle trajectories for various wall boundary conditions ($v^*_w = 3$, 1 and $A \times p^*_{in} = 3 \times 1$, 1×1) are shown for thin-channel and tublar modules. Trajectories are shown at four different elapsed time since the beginining of UF operations. At time, $t^* = 0$, the trajectory calculations are based on the flow-field described in previous section. As time of UF operation progresses, the particle layer builds up, resulting in added resistance to the permeate flow across the membrane. It is assumed that the porosity of the cake layer remains constant. Thus based on local steady state condition at each discrete time interval, the governing equations are solved with new wall boundary conditions for the next time interval. In Figures (6) and (7), trajectories are shown for the case of particle layer porosity, $\epsilon = 0.51$.

Any point (y^*,z^*) or (r^*,z^*) on the curves in Figures (6) and (7) shows that a particle starting at the inlet ($z^* = 0$), with half-height or radial position y^*or r^*, will follow a trajectory in the module which is determined by the hydrodynamics and wall flux conditions and will finally deposit on the membrane walls y^*or $r^* = 1$, at axial location z^*. For both modules, as the time of operations increases, the limiting particle trajectory curves move towards the membrane wall, which is due to increasing resistance of the particle layer on the membrane surface. As a consequence, the flux declines with time. It may be noted in Figures 6(a) and (c), the curves at $t^* = 0$, due to flow reversal, the locus of limiting trajectories are S-shaped. At later times , these curves change their shape to that of lower wall flux conditions. This is due to substantial decrease in wall permeation velocity, caused by the high initial particle deposition rates associated with high initial wall flux conditions.

Based on limiting particle trajectory calculations, the particle deposition rates as a function of time are shown in Figures (8) and (9) for thin-channel and tubular UF membrane modules with wall flux conditions, $v^*_w = 1$, 0.1 and $A \times p^*_{in} = 1 \times 1$, 0.1×1. Deposition rates are computed for three arbitrary cake porosity, $\epsilon = 0.51$, 0.30 and 0.15. For the same wall flux conditions, the particle deposition rates decrease rapidly with decreasing cake porosity as compared with that of the case of higher cake porosity. At low wall permeation flux conditions ($v^*_w = 0.1$ and $A \times p^*_{in} = 0.1 \times 1$) with high porosity ($\epsilon = 0.51$), the particle deposition rates essentially remain constant, as shown in Figures 8(b,d) and 9(b,d).

The average wall permeation flux is defined as the product of average permeation velocity and surface area. In Figures (10) and (11), the average wall permeation rates as a function of time are shown for thin-channel and tubular modules with wall flux conditions and particle layer porosity of that mentioned in Figures (8) and (9). Comparing Figures (10) and (11) with (8) and (9), it is clear that the particle deposition rates dictate the permeate flow rates and the permeate flux decline is very similar to the profiles of particle deposition rates for both thin-channel and tubular modules. Also, it is to be noted that due to high initial deposition rates, there is a rapid initial decline in permeate flow rates followed by a slower rate over the time of UF operations.

Model Varification with Experimental Data

As mentioned in the introduction of this paper, there is hardly any data reported in the literature on UF membrane fouling by particulate suspensions. Belfort and his

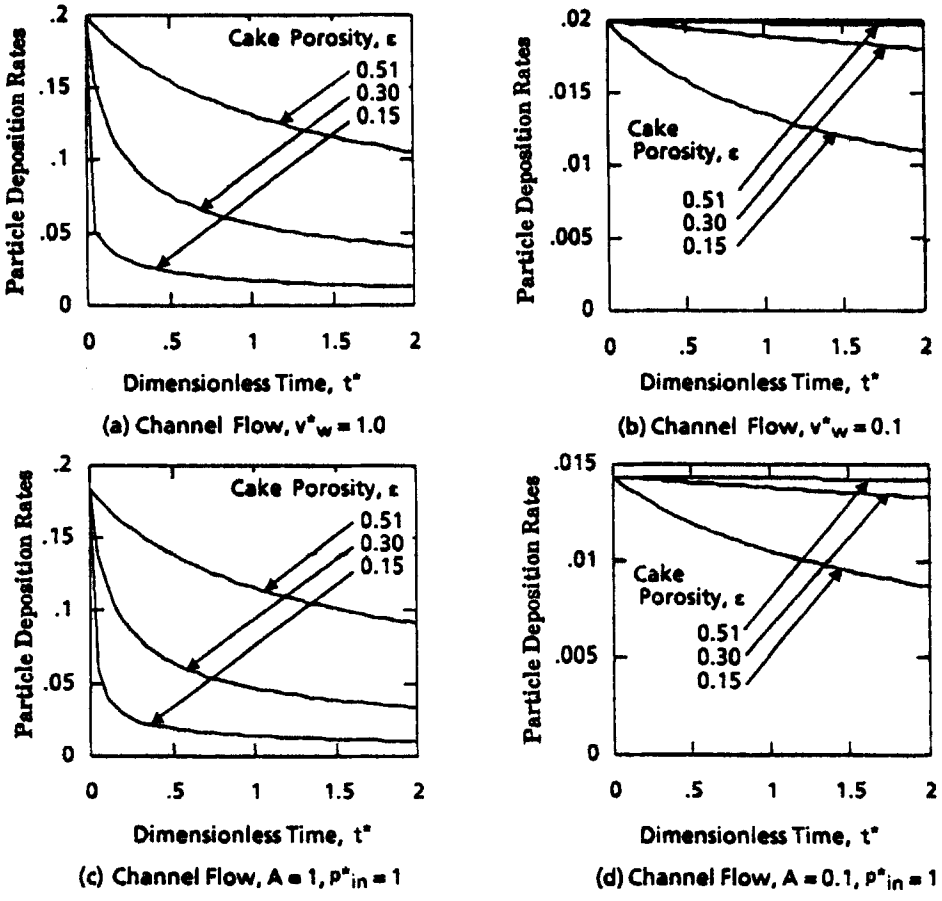

Figure 8: Effect of cake porosity on particle deposition rates as a function of time in a thin-channel UF module with fully developed inlet profile and initial flux conditions, (a) $v^*_w = 1$, (b) $v^*_w = 0.1$, (c) $v^*_w = A \times p^*_{in} = 1 \times 1$, and (d) $v^*_w = A \times p^*_{in} = 0.1 \times 1$.

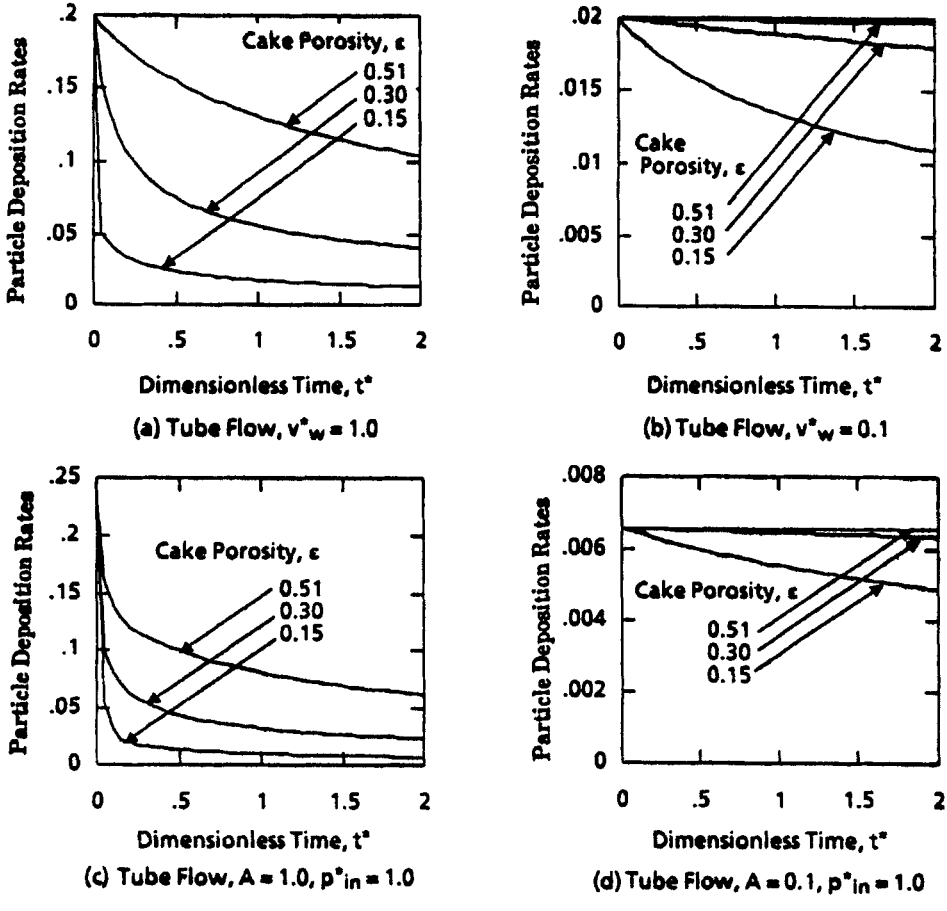

Figure 9: Effect of cake porosity on particle deposition rates as a function of time in a tubular UF module with fully developed inlet profile and initial flux conditions, (a) $v^*_w = 1$, (b) $v^*_w = 0.1$, (c) $v^*_w = A \times p^*_{in} = 1 \times 1$, and (d) $v^*_w = A \times p^*_{in} = 0.1 \times 1$.

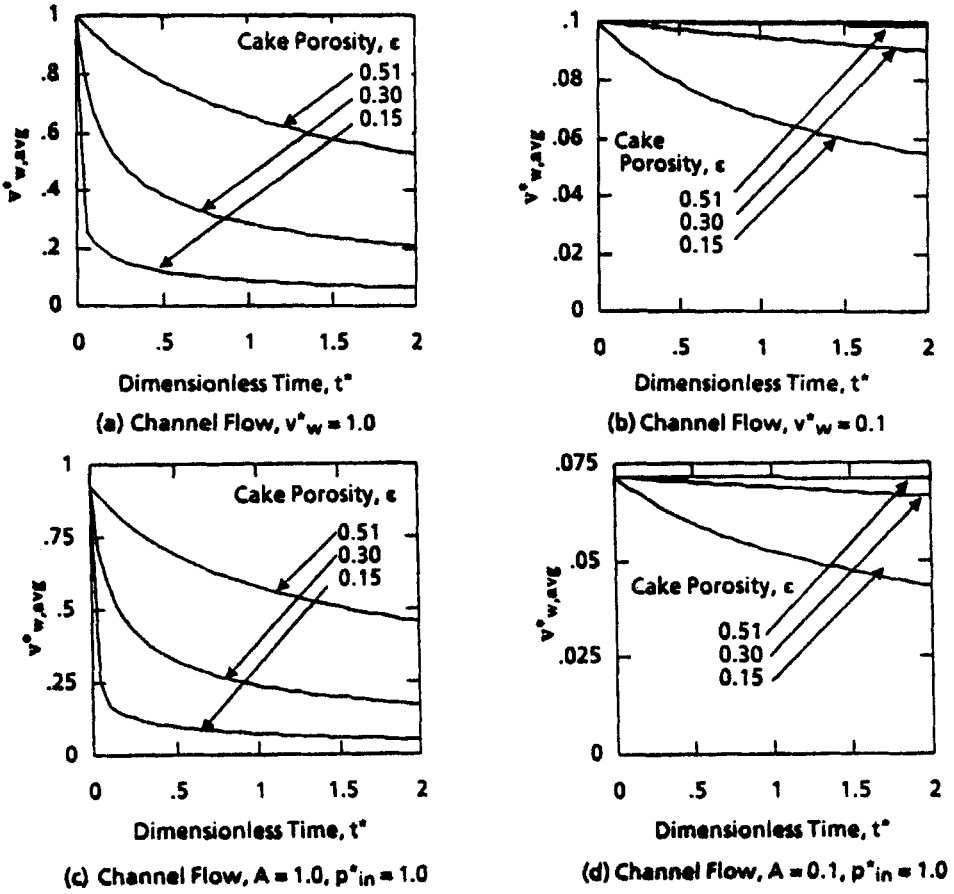

Figure 10: Effect of cake porosity on average permeate flow rates as a function of time in a thin-channel UF module with fully developed inlet profile and initial flux conditions, (a) $v^*_w = 1$, (b) $v^*_w = 0.1$, (c) $v^*_w = A \times p^*_{in} = 1 \times 1$, and (d) $v^*_w = A \times p^*_{in} = 0.1 \times 1$.

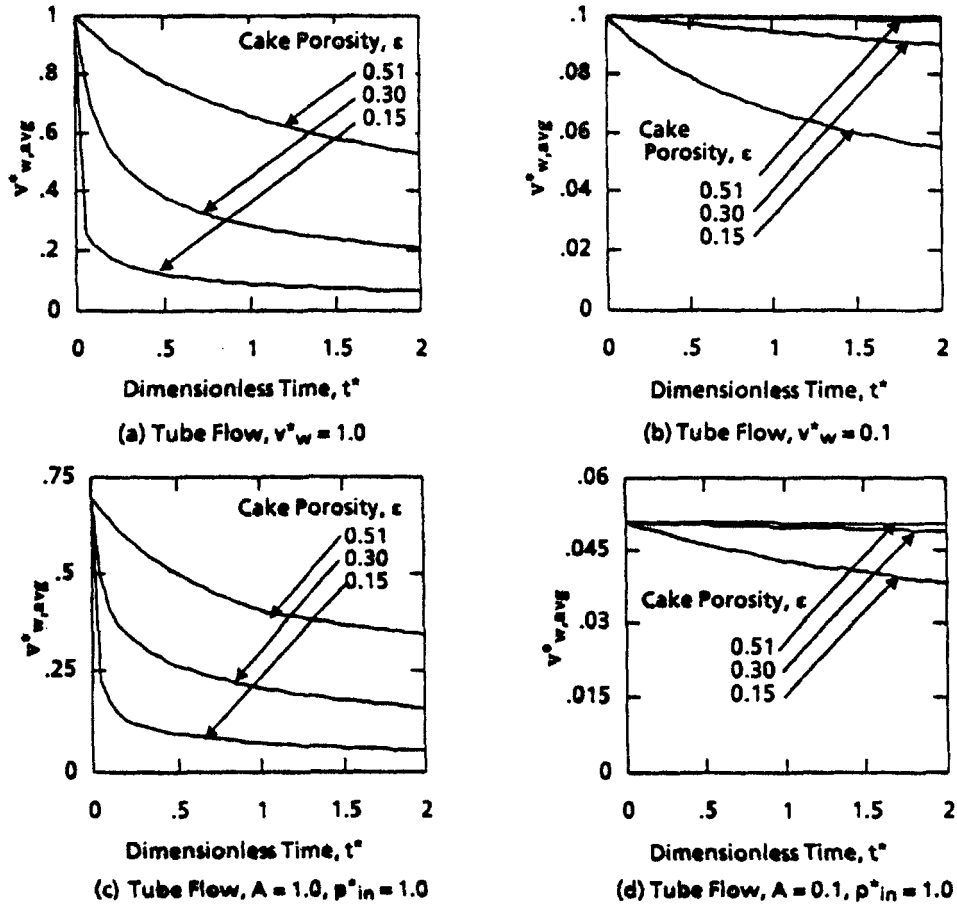

Figure 11: Effect of cake porosity on average permeate flow rates as a function of time in a tubular UF module with fully developed inlet profile and initial flux conditions, (a) $v^*_w = 1$, (b) $v^*_w = 0.1$, (c) $v^*_w = A \times p^*_{in} = 1 \times 1$, and (d) $v^*_w = A \times p^*_{in} = 0.1 \times 1$.

group (5,6), studied both theoretically and experimentally the migration of single spherical particles in thin-channel cells with one permeable wall. The system we modeled is slightly different (both wall permeable) from Belfort's model , however our trajectory calculation at low wall permeation flux conditions closely agree with that reported in their work. Due to non-availability of experimental data on particulate fouling in UF membranes, it is not possible to validate the model predictions. However, the trend observed in flux decline due to particulate fouling is similar to that one observes in the concentration polarization model. The authors are in the process of developing controlled UF experiments with dilute suspensions to measure flux decline, particle layer and membrane permeability using both inorganic and polymeric membranes. In a later paper, test results and model simulations will be reported.

CONCLUSIONS

From the simulation results on fouling thin-channel and tubular UF membrane modules by dilute suspensions, the following conclusions may be drawn:

- Inertial effects are important and under positive wall permeation flux, particles are encouraged to migrate towards the membrane wall, thus causing so-called *'membrane fouling'* by the particulates and dilute suspensions.
- Under identical flow conditions, a UF tubular module will foul at shorter axial length than in a thin-channel module.
- The extent of membrane fouling depends on the flow and the wall permeation flux conditions.
- Under high wall permeation flux conditions, both in tubular and thin-channel UF modules, the fouling occurs at shorter axial lengths
- In practice, UF modules operate in the range of $v^*_w < 1.0$. At this range, our simulations show that membrane fouling decrease rapidly with decreasing wall permeation flux conditions.
- At high initial wall permeation flux conditions, the product flux declines very rapidly at the beginning of operation for a given porosity of the deposited cake layer and then approach some assymtotic value at late times.

Inertial effects need to be considered in modeling UF/MF systems where concentration polarization by macromolecules or particles are important. If the inertial effects are not considered, then a pure concentration polarization model will underestimate the flux decline of the UF/MF membrane modules.

NOMENCLATURE

A	dimensionless membrane permeability, $(RkU^2_{0,m}/\nu^2 h)$
C_0, C^*	inlet particle concentration, (g/cm^3), dimensionless concentration, (C/C_0)
C_D	particle drag coefficient, dimensionless
d, d_p	tubular UF membrane module and particle diameters, (cm)
H	half-height of thin-channel UF membrane module, (cm)
h, h'	thickness of membrane wall and cake layer, (cm)
k, k'	permeability of membrane and cake layer, (cm^2)
p, p_0	pressure, inside and outside of UF module, (Pa)
p^*	dimensionless pressure, $([p-p_0]/\rho U^2_{0,m})$
R, r	radius of tubular module and radial direction
Re_p	particle Reynolds number

R_f	dimensionless resistances of cake layer, ($\nu^2 h'/kHU^2_{0,m}$)
R_m	dimensionless resistance of membrane wall, (1/A)
t, t^*	time, (s), dimensionless time, ($t\nu/H^2$ or $t\nu/R^2$)
u, u^*	axial velocity in z-direction, (cm/s), dimensionless axial velocity, ($u/U_{0,m}$)
$U_{0,m}$	mean velocity at the entrance, cm/s
v, v^*	transverse or radial velocity, (cm/s), dimensionless velocity, (Hv/ν or Rv/ν)
y, y^*	transverse or radial coordinate, normalized coordinate, (y/H or y/R)
z, z^*	axial direction, normalized coordinate, ($z\nu/H^2U_{m,0}$ or $z\nu/R^2U_{m,0}$)

Greek Symbols

ϵ	porosity of cake layer, dimensionless
Γ	particle deposition flux, dimensionless, defined in eqn (5)
ν	kinematic viscosity of fluid, (cm^2/s)
μ	viscosity of fluid, (g/cm s)
ρ, ρ_p	density of fluid, particle, (g/cm^3)

Subscripts

p	particles
s	starting condition for integration of equations (3) and (4)
w	conditions at wall or membrane surface
0, in	inlet condition

ACKNOWLEDGEMENTS

This work was supported by a grant from the Standard Oil of Ohio (SOHIO), Cleveland.

REFERENCES

1. M. Cheryan, *Ultrafiltration Hand Book*, Technomic Publishing Inc., Pa 17604 (1986).

2. R.L. Merson and D.N. Lee, "Prefiltration of cottage whey to reduce fouling of ultrafiltration membrane", *J. food Sci., 41*, 403-410 (1976).

3. A. Suki, A.G. Fane, and C.J.D. Fell, "Flux decline in protein ultrafiltration", *J. Membrane Sci., 21*, 269-283 (1984).

4. H. Reihanian, C.R. Robertson, and A.S. Michaels, "Mechanisms of polarisation and fouling of ultrafiltration membrane by proteins", *J. Membrane Sci., 16*, 237-258 (1983).

5. Belfort, G., R.J. Weigand and J.T. Mahar, , "Particulate membrane fouling and recent developments in fluid mechanics of dilute suspensions," in *Reverse Osmosis and Ultrafiltration, ACS Symposium Series No. 281*, S. Sourirajan and T. Matsuura (eds.), Amer. Chem. Soc., Washington D.C., 383-401 (1985).

6. Kleinstreuer, C. and G. Belfort, "Mathematical modeling of fluid flow and solute distribution in pressure-driven membrane modules," in *Synthetic Membrane Processes: fundamentals and water applications*, G. Belfort (ed.), Academic Press, 131-190 (1984).

7. J.A. Howell, and D. Velicangil, "Theoretical consideration of membrane fouling and its treatment with immobilized enzymes for protein ultrafiltration", *J. Appl. Polymer Sci., 27*, 21-32 (1982).

8. W.F. Leung and R.F. Probstein, "Low polarization in laminar ultrafiltration of macromolecules," *Ind. Eng. Chem. Fund., 18*, 274-278 (1979).

9. D.R. Trettin and M.R. Doshi, "Limiting flux in ultrafiltration of macromolecular solutions," *Chem. Eng. Commun., 4*, 507-522 (1980).

10. J. Gilron and D. Hasson, "Analysis of laminar flow precipitation fouling on reverse osmosis membranes," *Desalination, 60*, 9-24 (1986).

11. S. Ilias and R. Govind, "Fluid dynamics of dilute suspensions and fouling of tubular membrane modules," Paper accepted for publication, *J. Membrane Sci.*, (1988).